ACS APPLIED MATERIALS & INTERFACES

Research Article

www.acsami.org

Enhanced Electrochemical Performance of Highly Porous Supercapacitor Electrodes Based on Solution Processed Polyaniline Thin Films

Sunghun Cho, Kyoung-Hwan Shin, and Jyongsik Jang*

WCU Program of Chemical Convergence for Energy and Environment (C2E2), School of Chemical and Biological Engineering, College of Engineering, Seoul National University, Shinlimdong 56-1, Seoul 151-742, Korea

Supporting Information

ABSTRACT: Enhancement to the electrochemical performance of supercapacitor electrodes were realized by incorporating highly porous conductive polymer films prepared with solution-processed polyaniline. The resultant nanostructures contained characteristic pores measuring 30−150 nm. Such electrodes generated from a solution of polyaniline-camphorsulfonic acid (PANI/CSA) exhibited higher porosity and electro-catalytic activity than those generated from conventional PANI nanomaterials. These improvements were attributed to faster ion diffusion at the PANI electrode/electrolyte interface. The highest specific capacitance observed for a supercapacitor fabricated with a porous PANI electrode obtained was 361 F g^{-1} at 0.25 A g^{-1}, which is more than twice that of an equivalent electrode made with pristine PANI. Furthermore, supercapacitors made with highly porous PANI electrodes exhibited high electrochemical stability and rate performances.

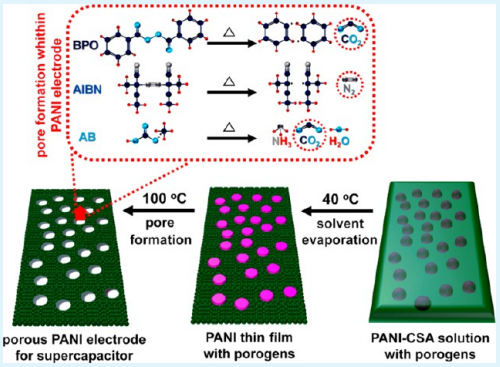

KEYWORDS: *polyaniline, thin film, conductive polymer solution, porous electrode, supercapacitor*

INTRODUCTION

Conductive polymer nanostructures have attracted a great deal of interest for use in energy applications because of several beneficial characteristics including tunable electrical properties, flexibility, and high processability from solution.[1,2] Solution-processable, conductive polymers, such as polyethylene(3,4-dioxythiophene):poly(4-styrenesulfonate) (PEDOT:PSS),[2−9] polyaniline-camphorsulfonic acid (PANI/CSA),[10−14] and polyaniline:poly(4-styrenesulfonate) (PANI:PSS),[15−17] have been widely investigated as electrode materials because they provide a facile and inexpensive way to form thin-film electrodes, which offer tunable thickness, high conductivity, and excellent optical transparency. Such systems have been used as electrode materials for various energy devices including chemical gas sensors, organic light-emitting diodes (OLEDs), electronic paper, and dye-sensitized solar cells (DSSCs). Furthermore, they have been studied as potential replacements for metals and transparent conductive oxide (TCO) films such as indium tin oxide (ITO) and fluorine-doped tin oxide (FTO).[2,14] While TCO films may crack after repeated bending, thin films of solution-processed, conductive polymers are seldom affected by repeated bending.

In particular, PANI has relatively high electrochemical and thermal stabilities and reversible pseudocapacitance, and PANI-based electrode materials have shown great potential for supercapacitor applications.[18−21] Various materials, such as 1D PANI nanomaterials, PANI/metal composites, and PANI/carbon composites,[22−32] have been fabricated as means of incorporating PANI-based electrode materials into supercapacitors. However, most of these exhibit low conductivity and poor processability from organic solvents, making them inadequate for most practical applications in high-performance supercapacitors. Compared to conventional PANI electrodes, electrodes generated from PANI/CSA solution boast two or three orders of magnitude greater conductivity.[12] In addition, PANI/CSA films deposited from solution adhere well to various substrates, including glass, metal, flexible plastic, and silicon, without any further treatment to ease their formation. While PANI/CSA appears to overcome the limitations of conventional PANI, the low surface area of PANI/CSA films limits their applicability in solar cells and supercapacitors. Electro-catalytic activity depends on the degree of contact between the electrode and the electrolyte and increases with the surface area of the electrode in most energy devices, including supercapacitors, solar cells, and Li-ion batteries.[26,33] Thus, a method for incorporating the porous structures into the solution-processable conductive polymer electrodes is highly desirable.

The present report describes a novel method for fabricating porous, highly conductive PANI thin films for use as working

Received: July 8, 2013
Accepted: August 28, 2013
Published: September 13, 2013

electrodes in a supercapacitor. Introducing thermally decomposing compounds such as benzoyl peroxide (BPO), azoisobutyronitrile (AIBN), and ammonium bicarbonate (AB) into conventional CSA-doped PANI solutions resulted in the formation of highly porous PANI thin films. These films have contained pores of 30−150 nm and exhibited significantly enhanced electro-catalytic activity relative to that of a pristine PANI thin film. These films were employed as electrode materials in a supercapacitor, with a maximum specific capacitance of 361 F g^{-1}.

EXPERIMENTAL SECTION

Materials. Aniline (99.0%), ammonium persulfate (APS, 98.0%), camphorsulfonic acid (CSA, 98.0%), benzoyl peroxide (BPO), azoisobutyronitrile (AIBN), and ammonium bicarbonate (AB) were purchased from Sigma-Aldrich (St. Louis, MO, U.S.A.). Hydrochloric acid (HCl, 35.0−37.0%), chloroform ($CHCl_3$), and ammonia solution (NH_3) were acquired from Samchun (Seoul, Korea). *m*-Cresol was obtained from Tokyo Chemical Industry (Tokyo, Japan). Distilled water was used as the solvent for the polymerization of aniline.

Synthesis of Porous PANI Thin Films for Use as Electrode Materials. PANI emeraldine salt (ES) powders were synthesized using a self-stabilized dispersion polymerization (SSDP) method based on chemical oxidation polymerization at −30 °C. Hydrogen chloride (HCl, Samchun, 0.1 mol) was introduced as a primary dopant into distilled water (30 mL). The aqueous anilinium ion solution was mixed with chloroform (Samchun, 60 mL). Aniline monomer (21 mmol) was added drop-wise to the as-prepared solution. The polymerization of aniline was performed using ammonium persulfate (APS, Aldrich, 2.4 g) as an oxidizing agent for 8 h at −30°C. The overall reaction progressed at the interface between the aqueous phase and chloroform. After washing with water, ethanol, and acetone, precipitates of greenish PANI ES were obtained. The primary dopant of PANI ES was removed by adding 0.5 M ammonia solution (NH_3, Samchun) as a reducing agent. The products were washed with ethanol and acetone to obtain brownish PANI emeraldine base (EB) powders. Secondary doping of the PANI EB powders was conducted with camphorsulfonic acid (CSA, Aldrich). PANI/CSA solutions, each containing a different porogen agent, were prepared by mixing secondary-doped PANI/CSA powders (0.04 g mL^{-1}) with either benzoyl peroxide (BPO, Aldrich, 2 mg mL^{-1}), azoisobutyronitrile (AIBN, Aldrich, 2 mg L^{-1}), or ammonium bicarbonate (AB, Aldrich, 2 mg mL^{-1}) in *m*-cresol/$CHCl_3$ (4:1, v/v) co-solvent. The *m*-cresol/$CHCl_3$ co-solvent solutions were sonicated for 24 h to increase the solubility of PANI/CSA powders within the solutions. The purified PANI/CSA solutions (0.025 mL) were drop-cast onto a stainless steel mesh (1.0 × 1.0 cm^2). This process resulted in a film thickness of about 10 μm. Two drying steps were used to obtain porous PANI thin-film electrodes. The first drying step (40 °C for 12 h) was designed to evaporate the *m*-cresol solvent. The second drying step (100 °C for 3 h) was used to induce thermal decomposition of BPO, AIBN, or AB within the PANI thin-film electrode.

Electrochemical Measurements. The electrochemical characteristics of the porous PANI thin-film electrodes were observed using a WBCS 3000 potentiostat/galvanostat (Wonatech, Korea). All electrochemical experiments were carried out in both three- and two-electrode cells. The three-electrode cells were evaluated under a 0.5 M H_2SO_4 electrolyte solution. PANI thin-films, deposited on stainless steel mesh (1.0 × 1.0 cm^2) served as working electrodes, and a platinum sheet (2.0 × 2.0 cm^2) was used as the counter electrode. The reference electrode was Ag/AgCl in saturated KCl solution. To build the two-electrode cell, gold foils were used as current collectors.[47] The purified PANI/CSA solutions (0.025 mL) were drop-cast onto the gold current collectors, resulting in a film thickness of about 10 μm. As-prepared PANI-coated current collectors were assembled with a glassy fibrous separator into sandwich-type cells. Cyclic voltammograms (CV) of porous electrodes were measured from 0 and 1.0 V at 20 mV s^{-1}. Galvanostatic charge/discharge experiments were performed by cycling the potential from 0 to 0.8 V at a current density of 0.25 A g^{-1}.

Instrumental Analyses. Surface images of the PANI thin-films were acquired with a field-emission scanning electron microscope (FE-SEM, JSM-6701F, JEOL, Japan) and an atomic force microscope (AFM, Innova SPM, Vecco, U.S.A.). Conductivities were measured using a four-point probe system (Mode systems Co, Korea) equipped with a current-source meter (Keithley 2400, Keithley Co., U.S.A.). X-ray diffractograms (XRDs) were measured with a powder X-ray diffractometer (M18XHF-SRA, MAC Science Co., U.S.A.). Ultraviolet/visible/near-Infrared (UV/VIS/NIR) and Fourier-transform infrared (FT-IR) spectra were measured on Lambda 35 and Frontier FT-IR spectrometers (PerkinElmer Inc., U.S.A.), respectively.

RESULTS AND DISCUSSION

The overall procedure for fabricating porous PANI supercapacitor electrodes from a solution of PANI/CSA is illustrated in Scheme 1. In the first step, highly conductive PANI

Scheme 1. Overall Procedure for Fabricating Porous PANI Supercapacitor Electrodes

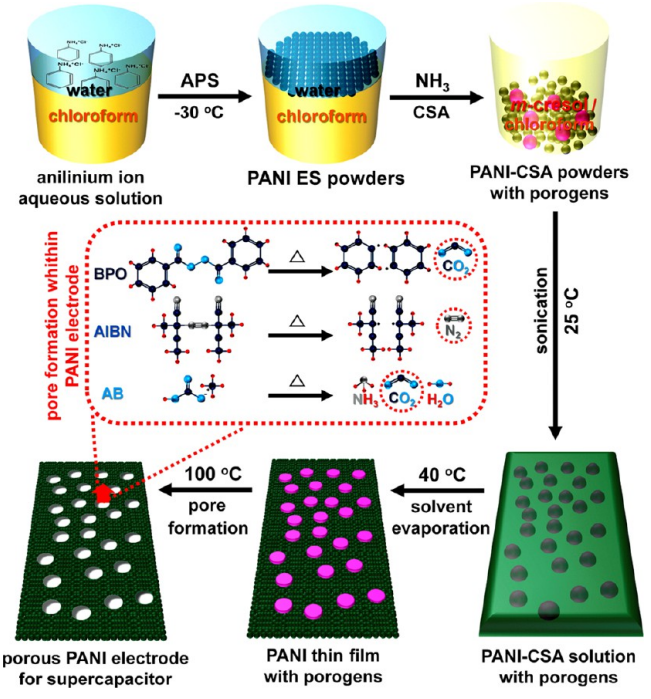

emeraldine salt (ES) powders were created using a self-stabilized dispersion polymerization (SSDP) method.[13] The SSDP method was designed to promote the *para*-direction polymerization at −30°C to achieve higher conductivity than the conventional methods. In this method, the protonated anilinium ions, which contain hydrophobic, hydrophilic, polar, and organic parts, act as interfacial stabilizers, allowing the excellent dispersion of organic phases into the aqueous medium.[12,13] The chloroform solvents separate insoluble oligomers and grown PANI chains in the aqueous phase, forming the PANI nanostructures, suppressing the undesirable side reactions, such as *ortho*-coupling and Michael reductive addition of aniline monomers. Importantly, the *para*-directed polymerization is induced by the SSDP method, which may result in the high quality PANI nanostructures with lower defects and enhanced charge transport properties compared to the conventional methods.[40,41] Ammonia (NH_3) was used as the reducing agent to remove the primary dopant (HCl) from

dx.doi.org/10.1021/am402702y | ACS Appl. Mater. Interfaces 2013, 5, 9186−9193

the PANI ES while the nitrogen atoms along the quinone diamine segment (−N═Q═N−) within the PANI structure for secondary doping. CSA was selected as a secondary dopant for the PANI emeraldine base (EB). Secondary doping changes the structure of PANI from a compact coil to an expanded coil.[10] Perforated and porous nanostructures were observed in both PANI ES and PANI/CSA powders (Supporting Information, Figure S1). Such porous structures may increase the solubility of the polymer in organic solvents such as *m*-cresol.[13] Furthermore, the nanostructures obtained from the SSDP method appeared to be grown radially, promoting the successive couplings of *para*-mode on benzene rings of aniline monomers, as mentioned above.[13] The sulfonic acid group ($-SO_3H$) of CSA forms a strong hydrogen bond with the hydroxyl group (−OH) of *m*-cresol, facilitated by the strong polarity and acidity of *m*-cresol. This strong compatibility of CSA molecules with the *m*-cresol solvents is a key reason for a dramatic increase in the conductivity of the PANI/CSA nanostructure.[10−14] Although such strong hydrogen bonds are associated with the high conductivity of PANI/CSA, the movement of CSA in the solvent can be suppressed. This can slow CSA doping at the −N═Q═N− unit of PANI EB. Chloroform is capable of forming a hydrogen bond with *m*-cresol, which indicates that more CSA molecules can form hydrogen bonds with $CHCl_3$ molecules. The increased interaction between CSA and $CHCl_3$, facilitates the diffusion of CSA in the system during aging. For these reasons, a co-solvent system composed of *m*-cresol/$CHCl_3$ (v/v = 4:1) was used for dissolution of the PANI/CSA powders. Sonication was used to increase the solubility of PANI/CSA powders in the *m*-cresol/$CHCl_3$ co-solvent. The high viscosity of the PANI/CSA solution, 1.53×10^3 centipoise (cP), is also attributable to the sonication-assisted dissolution of PANI/CSA in *m*-cresol/$CHCl_3$ solvents. This high viscosity of the PANI/CSA solution is associated with increased hydrodynamic volume and rapid changes in the molecular conformation of PANI/CSA from a compact coil to an expanded coil.[10] Taking these facts into account, the *m*-cresol/chloroform co-solvent system was necessary to achieve both high conductivity of the PANI/CSA nanostructures and their practical applicability in the capacitor device. After dissolution in organic solvent, the porous aggregates of PANI/CSA changed to film-type nanostructures with a flat surface composed of nanoscale grains with diameters of ∼40−60 nm. Thermally decomposing compounds, including BPO, AIBN, and AB, were added to the CSA-doped PANI as porogens, and the entire system was dissolved in the same solvent. As-prepared PANI/CSA solutions were cast as thin-film electrodes onto a stainless steel mesh. The high compatibility of PANI/CSA with various substrates can be attributed to the high surface polarity and wettability of the *m*-cresol solvent. Pore formation in the PANI thin films was induced thermally. Upon heating, gases (CO_2 from BPO and AB, and N_2 from AIBN) were emitted from the surface of the PANI electrode, generating pores of various diameters and shapes. The porous PANI thin films were presumed to benefit from the resulting enhancement of the surface area, which facilitates charge transfer and charge-discharge between the PANI electrode and the surrounding electrolyte.

Figure 1 shows field-emission scanning electron micrographs (FE-SEMs) of the PANI thin films. Grain size was ∼40−60 nm in both pristine film and those that had been made porous by BPO, AB, and AIBN (Figure 1a,c,e,g, respectively). Pore sizes

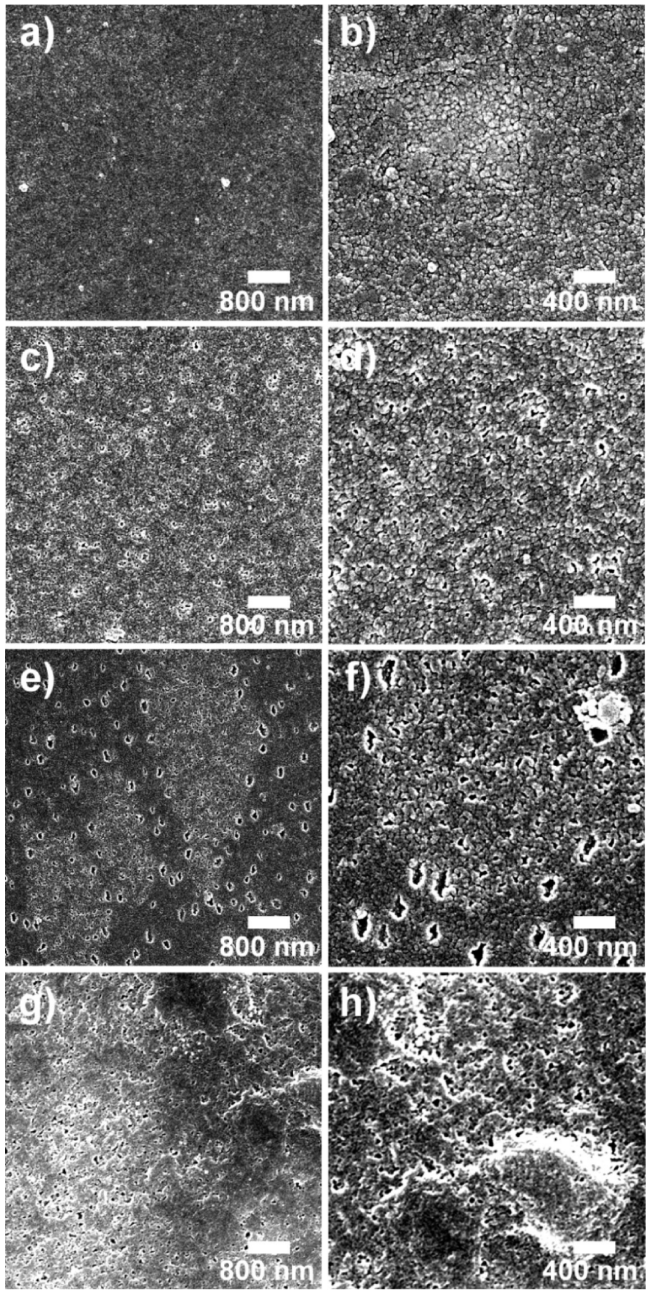

Figure 1. FE-SEM images of PANI thin films prepared by pore-forming process using different porogens: pristine (a, b), BPO (c, d), AIBN (e, f), and AB (g, h). Magnifications: ×20k (a, c, e, g) and ×40k (b, d, f, h).

in the BPO- and AB-PANI were ∼45 and 50 nm, respectively, indicating that CO_2 gas had been released by decomposition of the porogen (Figure 1d,h). The AIBN-PANI film had two types of pores with diameters of about 50 and 150 nm (Figure 1f). Pores 50 nm in diameter were found in specific regions at the film surface, while the larger pores were observed throughout the AIBN-PANI thin film (Figure 1e). These characteristics are thought to be due to the release of N_2 by the thermal decomposition of AIBN. Another factor affecting pore sizes may be associated with the decomposition rate (K_d) of the porogen agents. According to previous studies, the K_d value of AIBN is more than 10 times higher than the BPO at the same decomposition temperature.[42] This indicates that the AIBN is

more reactive than the BPO at the same temperature, resulting in wider pore size distributions and rougher surfaces. The AB molecules within the PANI thin-films are decomposed at a lower temperature (60 °C) compared to the BPO (70 °C) and AIBN (65 °C).[43] In addition, the NH_3 released from the thermal decomposition of the AB may also participate in the pore-forming reaction within the AB-PANI as well as the CO_2 gas.[46] Accordingly, the AB-PANI seemed to have rougher surfaces than the BPO- and AIBN-PANI. Based on these data, it is reasonable to assume that the use of all three porogens in a single film would result in entirely porous PANI thin films.

Atomic force microscopy (AFM) was used to study the surface morphologies of the PANI thin films (Figures 2 and 3).

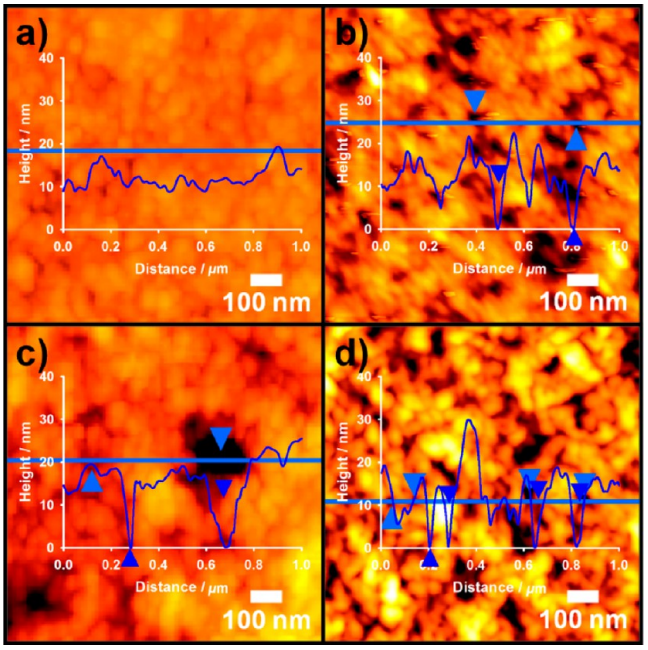

Figure 2. AFM images of PANI thin films with cross-sectional analyses (1 × 1 μm^2 scale): (a) pristine, (b) BPO-, (c) AIBN-, and (d) AB-PANI.

The AFM images of the PANI thin films in Figure 2 show grain and pore sizes that are consistent with those determined by FE-SEM. Figures 3a–c show the AFM images of the porous PANI thin films over a relatively wide area (10 × 10 μm^2). Highly porous nanostructures formed over the entire PANI surface. Interestingly, the AB-PANI seemed to have a rougher surface than did the BPO-PANI, although they exhibited similar pore sizes. Surface roughness (R_a) is a crucial factor affecting the electrical properties of PANI electrodes.[4,5] R_a values of the PANI electrodes increased as follows: pristine (2.37 nm) < BPO (4.05 nm) < AIBN (4.67 nm) < AB (5.83 nm). Compared to the pristine PANI, surface roughness increased significantly as a result of porogenesis. However, the conductive regions within the porous PANI were well-connected, regardless of which porogen was applied. Moreover, porogen decomposition within the PANI thin films is thought to have contributed further to the increase in surface roughness during solvent evaporation. The effective surface area of the electrode increases with increasing surface roughness, which facilitates faster electron transfer between the electrode and the surrounding electrolyte. However, increasing surface roughness may also reduce carrier mobility along the PANI thin film,

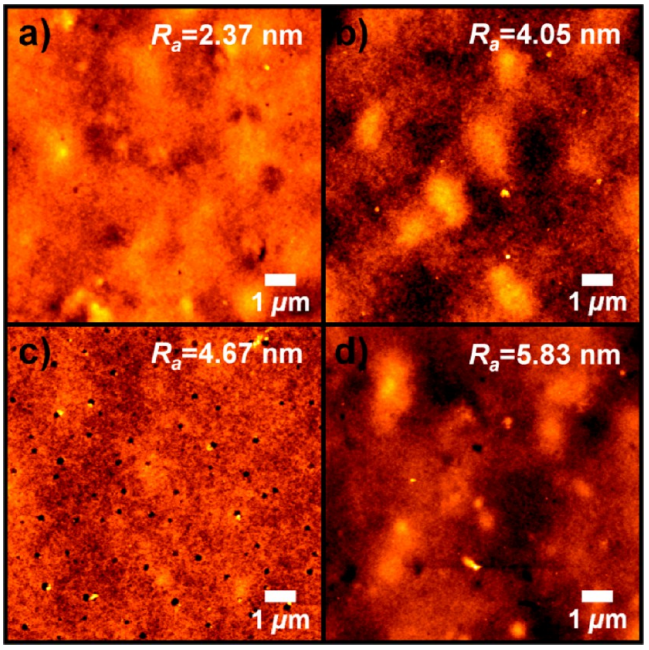

Figure 3. AFM images of PANI thin films after pore formation (10 × 10 μm^2 scale): (a) pristine, (b) BPO-, (c) AIBN-, and (d) AB-PANI.

Table 1. Relationship between Surface Roughness and Conductivity of PANI Thin Films Fabricated by Using Different Porogens

porogen	surface roughness (nm)[a]	conductivity (S cm^{-1})[a]	relative conductivity (σ_{rel})[b]
pristine	2.37	628.5	1.00
BPO	4.05	603.7	0.96
AIBN	4.67	596.8	0.95
AB	5.83	573.5	0.91

[a]PANI thin films with 10 μm thickness were deposited onto the substrate. [b]Relative conductivity compared to pristine PANI: $\sigma_{rel} = (\sigma)/(\sigma_0)\times 100$ (%).

which may lead to a decrease in conductivity. The observed dependence of conductivity on R_a is shown in Table 1. The conductivity of the PANI thin film is given by eq 1.

$$\sigma(\mathrm{S\ cm^{-1}}) = \frac{1}{\rho} = \frac{\ln 2}{\pi t}\left(\frac{1}{R}\right) \quad (1)$$

where ρ is the static resistivity, R is the sheet resistivity, and t is the thickness of the PANI film.[34,35] The conductivity of the electrode material is important for collecting currents within the capacitor device. The internal resistance of PANI/CSA is assumed to increase with increasing R_a. This increased internal resistance makes it more difficult to form conductive channels within the PANI thin film. Therefore, the electrical properties of PANI thin films are strongly affected by R_a. Jung et al.[36] reported that very small changes in surface roughness can enhance charge transport. Accordingly, R_a must be high enough to facilitate electro-catalytic activity at the PANI electrode/electrolyte surface. The results of the present study show only a small loss in conductivity caused by varying amounts of porogen. This indicates that the porous PANI films possessed

dx.doi.org/10.1021/am402702y | ACS Appl. Mater. Interfaces 2013, 5, 9186–9193

sustainable electrical properties. These data indicate that the BPO-, AB-, and AIBN-PANI films have high relative conductivities and large contact surface areas, making them suitable for use in electrochemical capacitors (Table 1).

The X-ray diffractograms (XRD) in Figure 4 show the changes in crystallinity associated with increasing porosity and

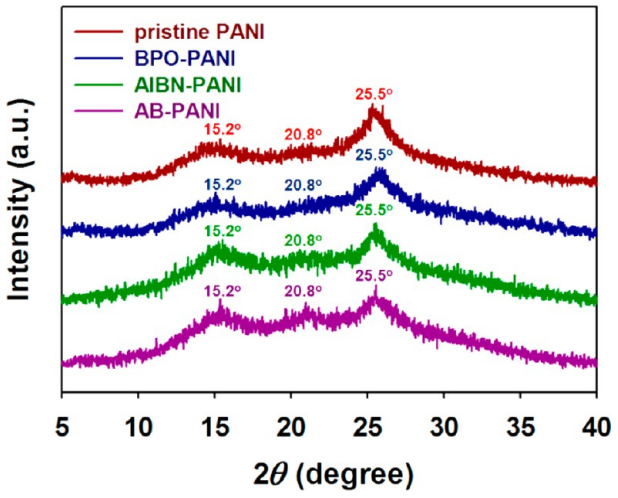

Figure 4. XRD patterns of PANI thin films fabricated by using different porogens.

surface roughness. Three distinctive peaks were observed with PANI/CSA at 2θ = 15.2°, 20.8°, and 25.5°. Previous reports,[10,12] have shown that when a PANI sample becomes more metallic, the broad background decreases while the relative intensity of these three peaks changes with increasing conductivity, the peaks at 15.2° and 20.8° decrease, and the peak at 25.5° increases. The diffractograms of the pristine, BPO-, AB-, and AIBN-PANI samples did not differ from each other and were similar to that of PANI/CSA.[10−12,14] The dominant peak at 25.5° is attributed to the degree of π-electron delocalization and the effective conjugation length of the PANI chains.[10] Increased delocalization results in better π-π^* interchain stacking within the PANI structure and higher conductivity.[12] These results suggest that the degree of crystallinity in PANI was preserved throughout the film-forming process, resulting in good agreement with measured electrical conductivities.

Utraviolet/visible/near-infrared (UV/VIS/NIR) and Fourier-transform infrared (FT-IR) spectroscopies were used to observe variation in the charge transport and chemical bonding properties of PANI thin films prepared with the different porogens (Figures 5 and 6). Figure 5 shows UV/VIS/NIR spectra of pristine and porous PANI thin films. Distinctive peaks at 320, 430, and 850 nm were assigned to π-π^* transitions of the benzenoid ring (−N═B═N−), a localized polaron to π^* transition, and a π to polaron transition, respectively. Free-carrier tails, which extended from 1000 nm to beyond 2000 nm, were observed in every UV/VIS/NIR spectrum of the PANI thin films.[10] The presence of free carriers is characteristic of delocalized polaron band structures possessing longer conjugation lengths within PANI/CSA. This type of delocalized band structure is assumed to originate from an expanded coil-like PANI structure. Solvation of dopant counterions is promoted by the diffusion of *m*-cresol molecules into the PANI/CSA chains, resulting in a local conformational

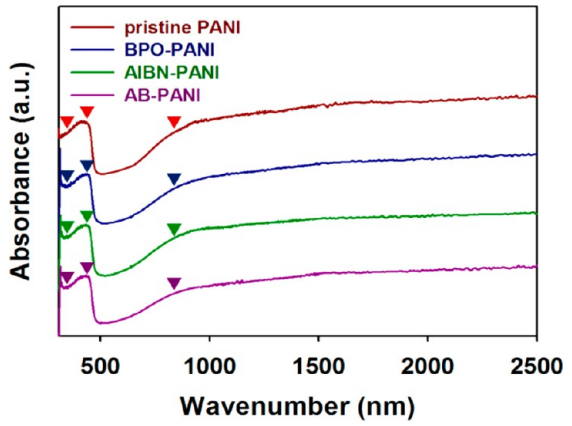

Figure 5. Distinctive bands in UV/VIS/NIR spectra of PANI thin films with different porogens.

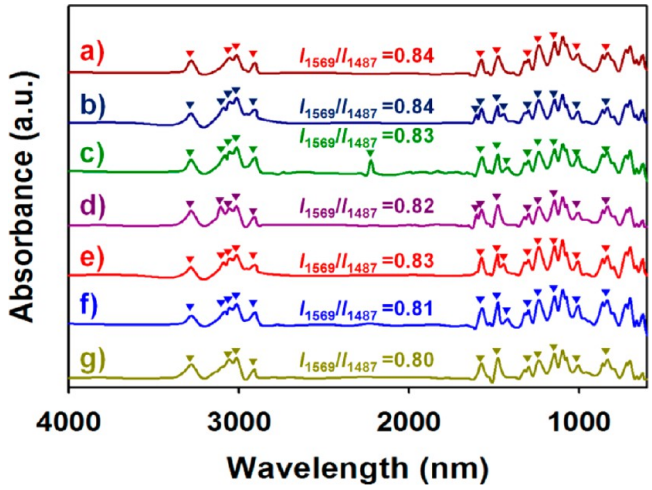

Figure 6. Distinctive bands in FT-IR spectra before pore formation of (a) pristine, (b) BPO-, (c) AIBN-, and (d) AB-PANI, and after pore formation of (e) BPO-, (f) AIBN-, and (g) AB-PANI.

change from a compact coil-like structure to an expanded coil-like one.[10] In PANI/CSA, this conformational change reduces twisting defects between polymer chains and elongates conjugation length. However, in the present study, no such changes occurred in pristine, BPO-, AB-, or AIBN-PANI. The charge transport properties of pristine PANI were retained in all of the porous PANI thin films.

To further investigate the changes in the chemical bonding properties associated with the pore formation, FT-IR spectra of the PANI/CSA nanostructures are shown in Figure 6. Several bands that are assigned to the porogen agents were found in the FT-IR spectra of nanostructures. Absorption bands at 3085 cm^{-1} and 3091 cm^{-1} in the spectra of the BPO- and AB-PANI, respectively, are assigned to C−H symmetric stretching of the phenyl rings and the methylene unit.[44,45] The peaks for C−C stretching of the BPO and AIBN appeared at 1443 cm^{-1} and 1421 cm^{-1}, respectively.[44,45] The band at 2226 cm^{-1} is attributed to the C−N stretching of the C−N═N−C unit.[45] The band at 1603 cm^{-1} in the spectra of the BPO-PANI is ascribed to asymmetric stretching of the C−O bonds, and the peak also appeared in the spectra of the AB-PANI.[44,46] The absorption band at 3120 cm^{-1} in the spectrum of the AB-PANI was due to the stretching of the NH_4^+.[46] After the pore-forming reactions within the thin films, the bands associated with the

dx.doi.org/10.1021/am402702y | ACS Appl. Mater. Interfaces 2013, 5, 9186−9193

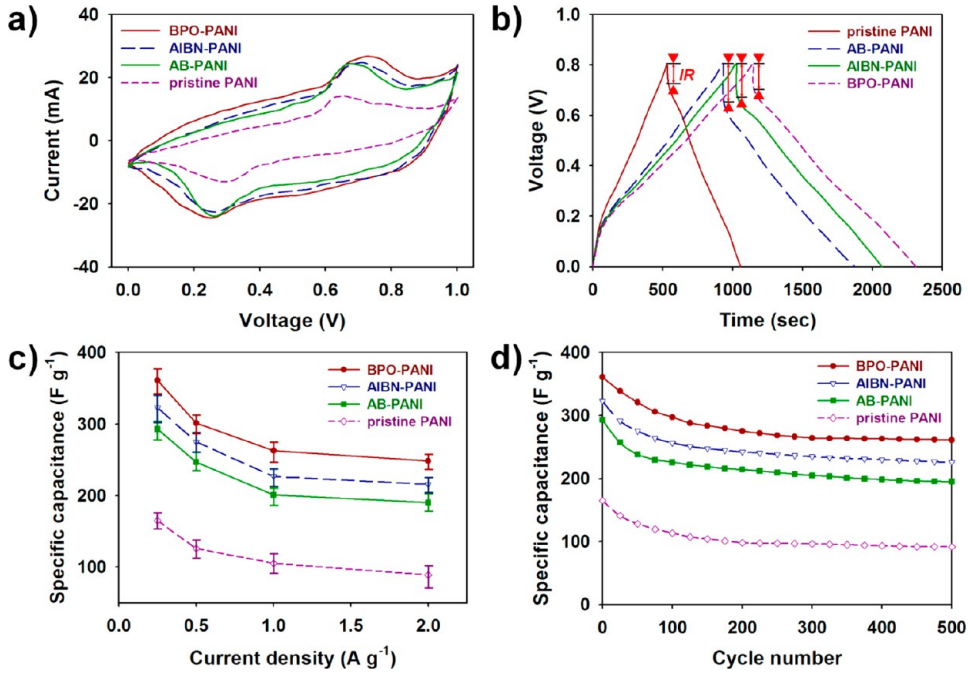

Figure 7. (a) Cyclic voltammograms of PANI thin-film electrodes scanned at 20 mV s^{-1} in 0.5 M H_2SO_4 electrolyte, (b) galvanostatic charge/discharge plots of PANI thin-film electrodes at current density of 0.25 A g^{-1}, (c) specific capacitances (C_m) of PANI thin-film electrodes at different current densities, and (d) cycling stability of PANI thin-film electrodes upon charge/discharge at a current density of 0.25 A g^{-1}. 0.025 mL of PANI solutions were used for forming thin films, resulting in a thickness of about 10 μm. The values were measured using a three-electrode system.

stretching of C−O, C−N, and NH_4^+ species were significantly reduced. These results indicate that the CO_2 (BPO and AB), N_2 (AIBN), and NH_3 (AB) gases were emitted from the PANI/CSA surface throughout the porogen decomposition. Several characteristic bands of PANI/CSA were observed in the FT-IR spectra of both nonporous and porous PANI samples. The band at 831 cm^{-1} was assigned to C−H out-of-plane bending of the 1,4-disubstituted rings. This band is also indicative of *para*-position coupling of the benzene rings of aniline. The bands of 1293 cm^{-1} and 3282 cm^{-1} were ascribed to C−N and N−H stretching of the secondary aromatic amine, respectively.[37−39] The absorption bands for C−H symmetric stretching of both the quinoid (−N═Q═N−) and the benzenoid unit (−N═B═N−) appeared at 2906, 3012, and 3058 cm^{-1}.[38] The bands at 1142 cm^{-1} and 1569 cm^{-1} were designated to C═C stretching of the −N═Q═N− unit. These two bands are also associated with delocalization of electrons within PANI/CSA. The spectra also contain bands at 1487 cm^{-1}, which are attributed to C═C stretching of the −N═B═N− unit. Note that the intensity ratio of the bands at 1569 cm^{-1} (I_{1569}) and 1487 cm^{-1} (I_{1487}) indicates the conjugation length and doping level of the PANI structure.[38] The I_{1569}/I_{1487} ratios of the pristine, BPO-, AIBN-, and AB-PANI thin films were almost the same, indicating that charge transport properties were not significantly affected by pore formation. The band at 1010 cm^{-1} can be ascribed to the sulfate anion ($-SO_3^-$) of the CSA dopant. The band at 1234 cm^{-1} originated from the bipolaron structure and may be indicative of the conducting, protonated form. These results demonstrate that the charge transport properties of pristine PANI, such as doping level and conjugation length, were preserved in the porous PANI thin films.

The electrochemical performance of cells based on porous PANI thin-film electrodes were evaluated by cyclic voltammetry (CV) and galvanostatic charge/discharge tests (Figure 7). Voltammograms of pristine and porous PANI electrodes were performed in 0.5 M sulfuric acid (H_2SO_4) from 0 to 1.0 V at a scan rate of 20 mV s^{-1} (Figure 7a). The anodic and cathodic peaks were attributed to leucomeraldine/emeraldine and emeraldine/pernigraniline transitions, respectively.[30,32] The electrochemical behavior of the PANI electrodes may be the result of Faradaic reactions at the PANI electrode/electrolyte surface. The BPO-PANI exhibited the highest electrochemical response. The area under the CV peaks obtained with pristine PANI electrodes was smaller than those of the BPO-, AIBN, and AB-PANI electrodes. The results suggest that the formation of porous structures within the PANI thin films increases the electrode surface area, which results in faster redox reactions between the PANI electrode and electrolyte. The cells based on PANI thin-film electrodes also exhibited symmetric charge/discharge curves, which implies that their electrochemical behavior originates from pseudocapacitance (Figure 7b).[28] The internal resistance (*IR*) of the PANI electrodes was estimated from the voltage drop at the onset of the discharge curves and was consistent with the conductivity of the thin films (Table 2).[29] The decrease in *IR* of the BPO-PANI supercapacitor was similar to that of the pristine PANI electrode. However, the BPO-PANI electrode exhibited a relatively longer discharge time, suggesting that the highly porous structure at the PANI surface leads to a larger capacity. Overall, discharge times were proportional to the specific capacitance of the PANI electrodes. The mass specific capacitance (C_m) of the PANI electrodes was measured using eq 2.

$$C_m = \frac{I\Delta t}{m\Delta V} \tag{2}$$

where I, Δt, m, and ΔV denote the constant discharge current, discharge time, total mass of the electrode, and voltage drop upon discharge, respectively.[29] The specific capacitances were

dx.doi.org/10.1021/am402702y | ACS Appl. Mater. Interfaces 2013, 5, 9186−9193

Table 2. Specific Capacitances, Internal Resistance Drops, and Discharging Times of PANI Thin-Film Electrodes Prepared by Different Porogens at a Current Density of 0.25 A g^{-1}

porogen	specific capacitance (F g^{-1})[c,d]	initial resistance (Ω)[c,d]	discharging time (sec)[c,d]
pristine	165	0.31	532
BPO	361	0.40	1149
AIBN	323	0.52	1028
AB	293	0.60	933

[c]0.025 mL of PANI solutions were used for forming thin films, resulting in a thickness of about 10 μm. [d]The values were measured using a three-electrode system.

361, 323, 293, and 165 F g^{-1} for the BPO-, AIBN-, AB-, and pristine-PANI electrodes, respectively, at a current density of 0.25 A g^{-1} (Table 2). To estimate the performance of the porous PANI in real supercapacitors, the electrochemical and galvanostatic charge/discharge performances of the porous PANI were evaluated using a two-electrode system (Supporting Information, Figure S2).[47,48] Although the specific capacitances and discharging times of the samples based on the two-electrode cells decreased from the values of the three-electrode cells, it was noteworthy that the porous PANI showed much better performances than the pristine PANI (Supporting Information, Table S1). The results obtained from the two-electrode system indicate that the porous structures play a key role in enhancing the capacitive performances of the PANI/CSA thin films. Rate performance was evaluated by performing charge/discharge cycles at different current densities (Figure 7c). The specific capacitances of the porous electrodes were higher than that of the pristine electrode. Specific capacitance decreased with increasing discharge current density. This decrease can be ascribed to diffusion of the supporting electrolyte. This suggests that a proportion of the electrode surface may be inaccessible at higher current densities. The BPO-, AB-, and AIBN-PANI electrodes maintained 69%, 67%, and 65% of their capacitance, respectively, with increasing current density while the pristine PANI film lost about 46% of its capacity in the same range of current densities. It is assumed that the porous structure facilitates their charge transfer during discharge. According to previous reports,[20,22] the long-term stability of conductive polymer electrodes is restricted by degradation caused by swelling and shrinkage that occurs during voltage cycling. The cyclic stability of the PANI thin-film electrodes was evaluated with galvanostatic charge/discharge cycles at a current density of 0.25 A g^{-1} (Figure 7d). After 500 such cycles, the specific capacitances of the BPO-, AIBN-, AB-, and pristine PANI electrodes decreased to 261, 226, 195, and 91 F g^{-1}, respectively, from their initial levels. Supporting Information, Figure S3 represents the specific capacitances of the PANI thin films with increased amounts (0.25 mL) of the samples with a film thickness of about 50 μm. On depositing more PANI/CSA solutions (0.25 mL) on the electrodes, the specific capacitances of the BPO-, AIBN-, AB-, and pristine PANI after the 500 cycles decreased to 217, 191, 163, and 65 F g^{-1}, respectively. Although the electrode surface seemed to become inaccessible with increasing mass loading of the electrode material, the increased mass loading only resulted in a small decrease in the specific capacitances of the samples.[47,48] The results suggest that these nanoporous architectures facilitate ion diffusion at the electrode/electrolyte surface while effectively minimizing the capacitance losses caused by degradation and shrinkage of the electrode materials.

CONCLUSIONS

A new strategy was developed to fabricate thin-film supercapacitors from porous, conductive polymer electrodes made from solutions of PANI/CSA. High porosity was generated by the incorporation of very small amounts of BPO, AIBN, and AB into the CSA-doped PANI. Relatively large improvements in electrochemical performance were attributed to the enhanced surface area of the porous polymer electrode, which results in enhanced contact between the electrodes and the surrounding electrolyte. Small increases in the surface roughness of porous PANI provided higher electro-catalytic activity and sustainable conductivities, resulting in low internal resistance and fast redox diffusion at the electrode/electrolyte surface. The specific capacitances of the porous PANI electrodes were as high as 361 and 213 F g^{-1} in the three-and two-electrode cells, respectively, which are significantly greater than those of pristine PANI. Furthermore, the porous PANI-based capacitors were electrochemically stable and boasted reasonable rate performance, making porous PANI one of the best electrode materials for high-performance capacitors. The procedure described herein provides a new means for producing porous, conductive polymer thin films for use as electrode materials in solar cells, Li-ion batteries, supercapacitors, and thin-film transistors.

ASSOCIATED CONTENT

Supporting Information

SEM images of PANI powders before secondary-doping and after secondary doping. This material is available free of charge via the Internet at http://pubs.acs.org.

AUTHOR INFORMATION

Corresponding Author

*E-mail: jsjang@plaza.snu.ac.kr.

Notes

The authors declare no competing financial interest.

ACKNOWLEDGMENTS

This work was supported by funding from the Center for Advanced Materials Processing under the 21C Frontier Programs of the Ministry of Knowledge Economy and the WCU (World Class University) program (R31-10013) and the Global Frontier R&D Program on Center for Multiscale Energy System funded by the National Research Foundation under the Ministry of Education, Science and Technology, Korea.

REFERENCES

(1) Gustafsson, B. G.; Cao, Y.; Treacy, G. M.; Klavetter, F.; Colaneri, N.; Heeger, A. J. *Nature* **1992**, *357*, 477−479.
(2) Xia, Y.; Ouyang, J. *J. Mater. Chem.* **2011**, *21*, 4927−4936.
(3) Burkhard, G. W.; McGehee, G. F.; Peumans, M. D. *Adv. Mater.* **2011**, *23*, 2905−2910.
(4) Wang, S.; Park, H. *J. Electroceram.* **2007**, *18*, 161−165.
(5) Jönsson, S. K. M.; Birgerson, J.; Crispin, X.; Greczynski, G.; Osikowicz, W.; van der Gon, A. W. D.; Salaneck, W. R.; Fahlman, M. *Synth. Met.* **2003**, *139*, 1−10.
(6) Rannou, P.; Nechtscheinl, M. *J. Chim. Phys.* **1998**, *95*, 1410−1413.
(7) Mauger, S. A.; Moulé, A. J. *Org. Electronics* **2011**, *12*, 1948−1956.
(8) Kim, Y.; Lee, J.; Kang, H.; Kim, G.; Kim, N.; Lee, K. *Sol. Energy Mater. Sol. Cells* **2012**, *98*, 39−45.

(9) Vosgueritchian, M.; Lipomi, D. J.; Bao, Z. *Adv. Funct. Mater.* **2012**, *22*, 421−428.
(10) MacDiarmid, A. G.; Epstein, A. J. *Synth. Met.* **1994**, *65*, 103−116.
(11) Pougeta, J. P.; Hsu, C.-H.; MacDiarmid, A. G.; Epstein, A. J. *Synth. Met.* **1995**, *69*, 119−120.
(12) Lee, K.; Cho, S.; Park, S. H.; Heeger, A. J.; Lee, C.-W.; Lee, S.-H. *Nature* **2006**, *441*, 65−68.
(13) Lee, S.; Lee, D.; Lee, K.; Lee, C. *Adv. Funct. Mater.* **2005**, *15*, 1495−1500.
(14) Lee, B.; Park, S.; Back, H.; Lee, K. *Adv. Funct. Mater.* **2011**, *21*, 487−493.
(15) Kang, Y.; Lee, M.; Rhee, S. *Synth. Met.* **1992**, *52*, 319−332.
(16) Ha, J.; Cho, J.; Jang, J. *Adv. Mater.* **2007**, *19*, 1772−1775.
(17) Jang, J.; Ha, J.; Kim, K. *Thin Solid Films.* **2008**, *516*, 3152−3156.
(18) Jang, J. *Adv. Polym. Sci.* **2006**, *199*, 189−259.
(19) Jang, J.; Ha, J.; Kim, S. *Macromol. Res.* **2007**, *15*, 154−159.
(20) Snook, G. A.; Kao, P.; Best, A. S. *J. Power Sources* **2011**, *196*, 1−12.
(21) Bose, S.; Kulia, T.; Mishra, A. K.; Rajasekar, R.; Kim, N.; Lee, J. *J. Mater. Chem.* **2012**, *22*, 767−784.
(22) Benlanger, D.; Ben, X.; Davey, J.; Uribe, F.; Gottesfeld, S. *J. Electrochem. Soc.* **2000**, *147*, 2923−2929.
(23) Ryu, K.; Kim, K.; Park, N.; Park, Y.; Chang, S. *J. Power Sources* **2002**, *103*, 305−309.
(24) Yang, M.; Cheng, B.; Song, H.; Chen, X. *Electrochim. Acta* **2010**, *55*, 7021−7027.
(25) Liu, Y.; Deng, R.; Weng, Z.; Liu, H. *J. Mater. Chem.* **2012**, *22*, 13619−13624.
(26) Hu, J.; Wang, H.; Huang, X. *Electrochim. Acta* **2012**, *74*, 98−104.
(27) Wang, D.-W.; Li, F.; Zhao, J.; Ren, W.; Chen, Z.-G.; Tan, J.; Wu, Z.-S.; Gentle, I.; Lu, G. Q.; Cheng, H.-M. *ACS Nano* **2009**, *3*, 1745−1752.
(28) Xu, J.; Wang, K.; Zu, S.-Z.; Han, B.-H.; Wei, Z. *ACS Nano* **2010**, *4*, 5019−5026.
(29) Wu, Q.; Xu, Y.; Yao, Z.; Liu, A.; Shi, G. *ACS Nano* **2010**, *4*, 1963−1970.
(30) Kumar, N. A.; Choi, H.; Shin, Y.; Chang, D.; Dai, L.; Baek, J. *ACS Nano* **2012**, *6*, 1715−1723.
(31) Shao, L.; Jeon, J.; Lutkenhaus, L. *Chem. Mater.* **2012**, *24*, 181−189.
(32) Park, H.; Kim, T.; Kang, M.; Lee, J.; Yoon, H. *ACS Nano* **2012**, *6*, 7624−7633.
(33) Luo, X.; Killard, A. J.; Smyth, M. R. *Chem.—Eur. J.* **2007**, *13*, 2138−2143.
(34) Skotheim, T. A.; Elsenbaumer, R. L.; Shacklette, L. W. In *Handbook of Conducting polymers*; Marcel Dekker, Inc.: New York, 1986; p 1.
(35) van der Paw, L. J. *Philips Technol. Rev.* **1958**, *20*, 220−224.
(36) Jung, Y.; Kline, R. J.; Fischer, D. A.; Lin, E. K.; Heeney, M.; McCulloch, I.; DeLongchamp, D. M. *Adv. Funct. Mater.* **2008**, *18*, 742−750.
(37) Stejskal, J.; Sapurina, I.; Trchová, M.; Prokeš, J.; Křivka, I.; Tobolková, E. *Macromolecules* **1998**, *31*, 2218−2222.
(38) Hatchett, D. W.; Josowicz, M.; Janata, J. *J. Phys. Chem. B* **1999**, *103*, 10992−10998.
(39) Curran, S. A.; Zhang, D.; Wondmagegn, W.; Blau, W. *Synth. Met.* **2006**, *156*, 482−487.
(40) Huang, J.; Kaner, R. B. *J. Am. Chem. Soc.* **2004**, *126*, 851−855.
(41) Stejskal, J.; Gilbert, R. G. *Pure Appl. Chem.* **2002**, *74*, 857−867.
(42) Brandrup, J.; Immergut, E. H.; Grulke, E. A. In *Polymer Handbook*; John Wiley, Inc.: New York, 1999; Vol. 2, pp 2−69.
(43) Shale, C. C.; Simpson, D. G.; Lewis, P. S. *Chem. Eng. Prog. Symp. Ser.* **1971**, *67*, 52−58.
(44) Radziszewski, J. G.; Nimlos, M. R.; Winter, P. R.; Ellison, G. B. *J. Am. Chem. Soc.* **1996**, *118*, 7400−7401.
(45) Pabin-Szafko, B.; Wisniewska, E.; Czech, Z. *J. Chem. Chem. Technol.* **2009**, *3*, 101−106.
(46) Lee, H. S.; Ha, T. H.; Kim, K. K. *Mater. Chem. Phys.* **2005**, *93*, 376−382.
(47) Stoller, M. D.; Ruoff, R. S. *Energy Environ. Sci.* **2010**, *3*, 1294−1301.
(48) Gogotsi, Y.; Simon, P. *Science* **2011**, *334*, 917−918.